ELSEVIER

Journal of Power Sources 104 (2002) 157–168

JOURNAL OF POWER SOURCES

www.elsevier.com/locate/jpowsour

Electrochemical characterization of cobalt-encapsulated nickel as cathodes for MCFC

Anand Durairajan, Hector Colon-Mercado, Bala Haran, Ralph White, Branko Popov*

Department of Chemical Engineering, University of South Carolina, Columbia, SC 29208, USA

Received 2 August 2001; accepted 8 August 2001

Abstract

The stability of the NiO cathodes in molten carbonate fuel cell (MCFC) has been improved through microencapsulation of the NiO cathode with nanostructured Co. Cobalt was deposited on the NiO cathode using an electroless deposition process. The electrochemical oxidation behavior of the Co-coated electrodes is similar to that of the bare NiO cathode. The cobalt-coated electrodes have a lower solubility in the molten carbonate melt when compared to bare nickel oxide electrodes in the presence of cathode gas. The solubility decreased more than 50% due to microencapsulation with cobalt. The thermal oxidation rate was also lower in case of the cobalt-encapsulated electrode. Impedance data from the modified electrode indicate that the oxygen reduction reaction depended inversely on the CO_2 and directly on the oxygen partial pressures respectively suggesting a similar reaction mechanism to that of nickel oxide. The results indicated that cobalt-encapsulated NiO is a viable solution in the development of alternate cathodes for MCFC applications.

Keywords: Cobalt; Electroless plating; Molten carbonate; Fuel cell; Microencapsulation; Dissolution

1. Introduction

The molten carbonate fuel cell (MCFC), operating at a temperature of 650 °C, has been under intensive development for the last few decades as a second-generation fuel cell [1,2]. Significant advances have been done in addressing design issues resulting in the development of prototype MCFC power generators. However, several hurdles remain before commercialization of MCFC can be realized. The primary challenge remains in the proper selection of materials for the cathode and current collector. Current state-of-art [3] relies on NiO cathodes fabricated from Ni powder. However, during cell operation, nickel oxide dissolves in the electrolyte [4] and does not satisfy long-term stability criteria [5]. Nickel oxide reacts with CO_2 present in the electrolyte according to an acidic dissolution mechanism

$$NiO + CO_2 \rightarrow Ni^{2+} + {CO_3}^{2-}$$

The dissolved nickel remains in equilibrium with the NiO cathode. Simultaneously, the Ni^{2+} cation diffuses to the anode side of the electrolyte and is then reduced in the hydrogen atmosphere to metallic nickel. The diffusion of Ni^{2+} cation fuels more dissolution of nickel from the cathode. Continued deposition of Ni in the anode region eventually leads to a short circuit between the anode and cathode. The dissolution is accelerated under higher CO_2 partial pressure and results in lowering the operating life of the cell. Apart from this, cathode dissolution results in loss of active material and in decrease of the active surface area available for the oxygen reduction reaction (cathodic reaction) leading to degradation in fuel cell performance.

Current state-of-art on solving the Ni dissolution problem is focused on varying the molten salt constituents [6,7] or using alternate cathode materials [8–10]. More basic molten carbonate melts such as Li/Na carbonate eutectic have been used to decrease the Ni dissolution rate in the melt [6,7]. Alkaline earth metal salts based on Ba or Sr have also been used as additives to increase the basicity of the melt. However, using more basic molten carbonate melts only partially solves the problem, since these melts decrease the NiO dissolution rate by 10–15% only [6,7].

The other approach to counter the nickel dissolution problem is to either modify NiO or to identify alternate cathode materials, which have longer life in the melt. Alternate electrodes should have good electronic conductivity, chemical stability and proper microstructure for use as MCFC cathodes. $LiFeO_2$ and $LiCoO_2$ offered initial promise as replacement material for NiO cathodes [8–10]. However,

* Corresponding author. Tel.: +1-803-777-7314; fax: +1-803-777-8265.
E-mail address: popov@engr.sc.edu (B. Popov).

0378-7753/02/$ – see front matter
PII: S0378-7753(01)00972-7

the exchange current density for oxygen reduction reaction on $LiFeO_2$ is about two orders of magnitude lower than that on NiO. Thus, the slow kinetics for oxygen reduction limits the possibilities for further improvement of cathodes based on this material. $LiCoO_2$ is more stable than NiO in alkaline environment [8]. However, $LiCoO_2$ is less electronically conductive than NiO and is more expensive than NiO. Other choices for cathode materials have failed because of their low electronic conductivity or poor oxygen reduction kinetics. This being the case, surface modification of NiO with more resistant materials is being considered as the more viable alternative.

Based on previous investigations [11–15] cobalt has been chosen to modify the surface of the NiO cathode and reduce its dissolution. Previous investigators have attempted to modify the surface of NiO with Co through other approaches. Fukui et al. [11,12] and Zhang et al. [13] studied the effect of cobalt coating on nickel oxide particles used as cathodes in MCFC. Ni particles were covered with lithiated Co and Ni solid solution [12] or by CoO particles mechanically [11]. Composites made of the Ni–CoO particles showed better corrosion resistance as compared to that of conventional NiO in Li–K carbonate melt. However, polarization studies of the Ni–CoO composite were not reported. Kuk et al. prepared $LiCoO_2$-coated NiO cathode using two different techniques: by a PVA assisted sol–gel method [14] and by electroplating [15]. They found that the modified electrode performed better than the bare NiO in both electrochemical and dissolution studies.

Microencapsulation offers an easier and consistent way of coating the substrate with amorphous layers [16]. The objective of this study is to characterize the electrochemical and corrosion properties of microencapsulated NiO with Co as a cathode material in MCFC. A variety of electrochemical and physical characterization techniques have been used to study the performance of the Co–NiO composite.

2. Experimental

Porous nickel cathode was made by a tape casting and sintering process. Nickel (Aldrich) particles were ground and sieved to obtain uniform particles of size 3–5 μm. The tape casting slurry was prepared by ball milling nickel powder in water with suitable binder (PVA) and plasticizer (glycerol). The ball milling was done in two steps. At the first step, 50 g of nickel powder were added to 5 g of PVA (PVA liquid 15 wt.%) and 1 g of defoamer (Airdefoam™ 60, Air Products). The ingredients were mixed thoroughly with 15 g of water and the slurry was ball milled for 3 h in order to break the weak agglomerates. Next, 9 g of glycerol was added to the above suspension and the resulting slurry was ball milled for an additional 3 h. The slurry was then slightly warmed (50 °C) and degassed using a ROTOVAP® evaporator. The slurry was cooled and then cast using a doctor blade assembly over a glass plate coated with silicone oil. The drying was performed slowly at room temperature for about 48 h. The cast plate nickel tape was then stripped off gently from the glass plate and stored.

Prior to cobalt coating Ni tapes were activated in a solution of 20 g/l sodium hypophosphite at 90 °C. Subsequent to activation the deposition was carried out with moderate stirring at 80–85 °C in 20 g/l cobalt sulphate, 20 g/l sodium hypophosphite, 50 g/l sodium citrate and 40 g/l ammonium chloride for 1 h. In addition to the above constituents, NH_4OH was added periodically during deposition to maintain the pH between 8.5 and 9.5. The pH dropped below 9 frequently during deposition indicating that cobalt deposition on the alloy surface was proceeding. The deposition was terminated once the pH remained constant indicating the absence of cobalt in the solution. The cobalt-encapsulated nickel tape was rinsed with deionized water, dried at 65 °C for 4 h and later sintered at 800 °C in air for 2 h. This was done to remove all decomposable material, which could have been incorporated into the Ni laminate during Co deposition.

In situ oxidation of nickel and cobalt-encapsulated nickel electrodes were studied using a three-electrode half-cell. The working electrode was made of circular disc electrodes cut from sintered metal tapes and spot welded with a gold wire. Gold was used as the counter electrode and Au/$(2CO_2 + 1O_2)$ served as the reference electrode. The reference gas flow rate was maintained at 10 cm^3/min. Oxidant gas with a composition of 30% CO_2 and 70% air (National Welders) was directly purged into the carbonate melt through an alumina tube. The open circuit potential studies were done using an EG&G PAR Model 273 potentiostat interfaced with a computer.

The electrochemical studies were done in a 3 cm^2 lab cell shown in Fig. 1. Nickel and cobalt-encapsulated nickel were used as the working and counter electrodes. $(Li_{0.62}K_{0.38})_2CO_3$ eutectic embedded in a $LiAlO_2$ matrix was used as the electrolyte. Polarization studies were done using an oxidant gas composition of 70% air and 30% CO_2. Two oxygen reference electrodes ($Au/CO_2/O_2$) connected to the electrolyte tile with a salt bridge (50% $(Li_{0.62}K_{0.38})_2CO_3$ + 50% $LiAlO_2$) were used to monitor the polarization of cathode.

Electrochemical impedance spectroscopic studies were performed using a Model 1255 Schlumberger Frequency Analyzer. The electrode was stable during the experiments and its open circuit potential changed less than 1 mV. The impedance data generally covered a frequency range of 1 mHz–100 kHz. A sinusoidal ac voltage signal varying by ±5 mV was applied in all cases. Scanning electron microscope (SEM) was used to study the microstructure of the specimens.

Thermogravimetric analysis (TGA) was employed to investigate the thermal oxidation behavior of both cobalt-encapsulated and bare nickel electrodes in the presence of cathode gas conditions. The oxidation behavior was studied both in the presence and absence of the carbonate melt.

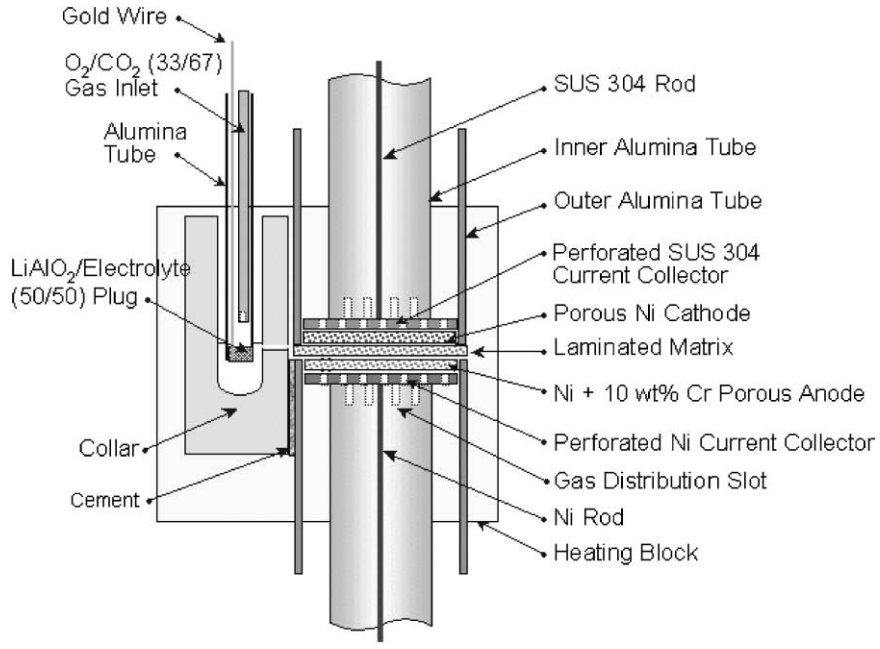

Fig. 1. Schematic diagram of a 3 cm^2 electrochemical fuel cell. Au/($2CO_2 + 1O_2$) reference electrode with a salt bridge was used for measuring cathode and anode potential during polarization studies.

In order to determine the solubility of nickel and cobalt-encapsulated nickel electrodes in molten carbonate, pot tests were carried out under cathode gas conditions. Pellet electrodes of 2.5 cm diameter were cut out from sintered nickel and cobalt-encapsulated nickel tapes. They were weighed and carefully dropped inside an alumina crucible containing 100 g of molten carbonate ($Li_2CO_3/K_2CO_3 = 62/38$) at 650 °C. Cathode gas (30% CO_2/70% air) was bubbled through the carbonate melt using alumina tubes. About 0.2 g of molten carbonate was taken from the melt approximately every 6 h up to 200 h using an alumina rod. The molten carbonate sample was dissolved in 10% dilute acetic acid. Atomic absorption (AA) spectroscopy was used to analyze the concentration of dissolved nickel and cobalt.

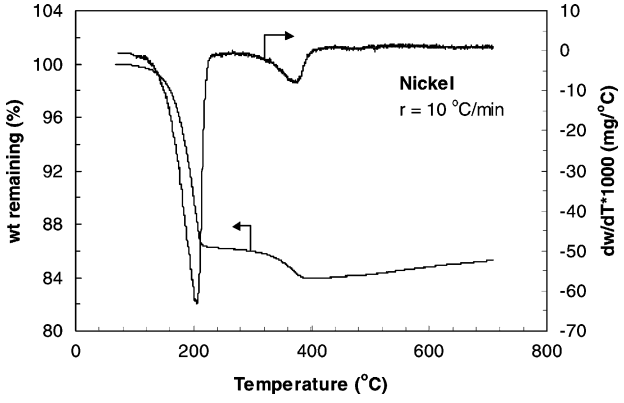

Fig. 2. Thermogravimetric analysis (TGA) of an aqueous nickel tape.

3. Results and discussion

3.1. Sintering

Sintering of the tape casted electrodes influences the cathode pore structure and thereby affects its electrochemical performance. TGA was done to determine the optimum heat treatment schedule for sintering. A typical TGA curve for green nickel tape is shown in Fig. 2. The as cast Ni tape was preheated at 120 °C for 12 h in order to remove all the water in the tape. TGA analysis was done by heating the sample from 100 to 650 °C at a rate of 10 °C/min. A steep reduction in weight (15 wt.%) is seen on heating the sample to 200 °C due to the removal of the binder. A secondary weight loss (5 wt.%) is noticed between 300 and 400 °C due to the removal of plasticizer. The removal of all volatile and decomposable organic matter is completed below 400 °C. On heating the sample above 400 °C, oxidation of nickel surface takes place. The total weight loss varies between 15 and 20 wt.% depending upon the binder and plasticizer contents in the green tapes. Since, Ni is oxidized beyond 400 °C, it is critical to heat the sample in a reducing atmosphere to prevent oxidation during sintering. Further, the rate of heating should be very slow initially to ensure complete burn out of binder and plasticizer. Based on the above TGA analysis, the following heating pattern was used for sintering the electrodes: (i) green tapes which were cut out to specific area (10 cm × 10 cm) were initially heated from room temperature to 130 °C at a rate of 1 °C/min in nitrogen atmosphere, (ii) in the second step the temperature was held at 130 °C for 10 h, (iii) next, the temperature was raised to 230 °C at a rate of 1 °C/min in nitrogen atmosphere, (iv)

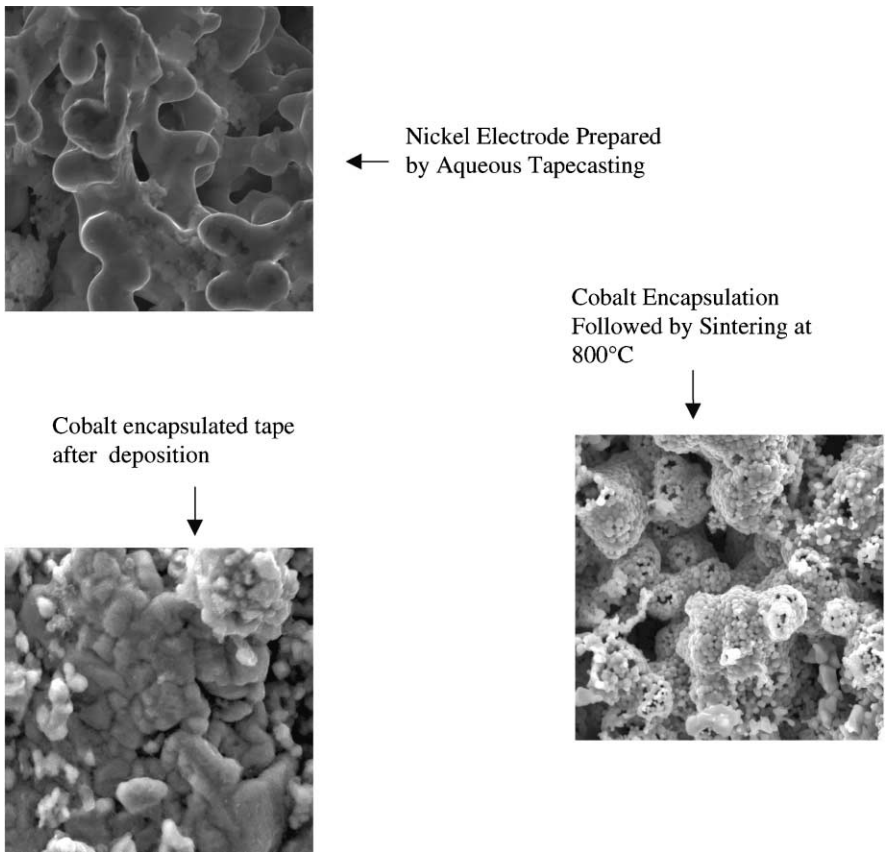

Fig. 3. SEM photographs of bare and cobalt-microencapsulated nickel electrodes obtained by tape casting and sintering.

the temperature was held at 230 °C for 2 h, (v) next the temperature was raised to 400 °C at 1 °C/min in nitrogen atmosphere, (vi) next, the temperature was maintained at 400 °C for 2 h, (vii) the temperature was raised to 800 °C at 1 °C/min in hydrogen atmosphere, (viii) the temperature was hold at 800 °C for 1 h and (ix) in the last step the sample was cooled to room temperature using a cooling rate of 1 °C/min in hydrogen atmosphere.

3.2. Scanning electron micrograph

Fig. 3 shows the SEM images of Ni and cobalt-encapsulated nickel electrodes prepared by the above sintering procedure. Cobalt microencapsulation leads to the formation of amorphous layers of cobalt over the entire microstructure of nickel tape. On heating the sample to 800 °C, the volatile substances included during the cobalt microencapsulation process decomposed giving rise to a porous Co–Ni composite electrode. The primary particle size according to Fig. 3 for nickel electrodes was in the range of 0.5–4 μm. Subsequent to Co encapsulation and sintering in air, the particles tend to agglomerate together. Detailed pore volume distribution analysis needs to be carried out to comment on the actual porosity and pore size distribution. The morphological difference between nickel and cobalt-encapsulated nickel can be attributed to the cobalt deposited over the nickel surface and the additional sintering done on the sample.

3.3. Vicker's hardness test

The MCFC cathodes are typically nickel tapes prepared by either tape casting followed by sintering or loose powder sintering process in hydrogen atmosphere so as to keep it from oxidizing. The nickel tape is then in situ oxidized in the molten carbonate under cathode gas conditions to form NiO. In situ oxidizing is believed to be beneficial in terms of improved hardness and the pore structure of the substrate. Cobalt-encapsulated cathodes were prepared using ex situ oxidation and therefore have to be characterized for hardness. A Vickers hardness indenter was used to indent the cobalt-encapsulated and bare nickel tapes with a diamond tip. The physical deformation that happened during the indendation process was observed under a microscope and the dimensions of the depression was marked. Vickers hardess number (VHN) [17] was calculated based on the observations made on the indent using the formula

$$\mathrm{VHN} = \frac{2P}{d^2}\sin\left(\frac{\alpha}{2}\right)$$

where d is the diagonal length left by the diamond shaped pyramid indenter. The angle between the phases of the

Table 1
Vickers hardness number (VHN) calculated for the Ni (sintered in H_2 atmosphere) and Co–NiO (sintered in air) tapes

Material	P (kg)	d (mm)	VHN (kg/mm^2)
Ni	200	6.2×10^{-4}	9.646×10^{8}
Co-coated Ni	200	4.7×10^{-4}	1.678×10^{9}

pyramid is $\alpha = 136^{\circ}$. P is the load used in kilograms and the units of d are in millimetre. VHN was calculated for the Ni (sintered under H_2 atmosphere) and cobalt-coated nickel (sintered in air) cathodes. Table 1 gives the applied load, indent observed and the VHN in case of Ni and Co–NiO. Cobalt-coated nickel cathode shows a higher VHN value than for nickel cathode indicating that the Co coating improves the hardness of the Ni tapes.

3.4. Stability tests

The short-term stability of cobalt-encapsulated and bare nickel in molten carbonate eutectic were determined using pot tests. AA was used to analyze the dissolved nickel and cobalt in the melt. Fig. 4 shows the results of AA analysis on the amount of dissolved nickel and cobalt in the carbonate melt as a function of time. As shown in the plot, the rate of dissolution of Ni^{2+} was significantly higher in case of bare nickel when compared to that of cobalt-microencapsulated nickel. Fukui et al. [11] prepared Co-coated NiO composites by a mechanical compaction technique. They found that the Ni dissolution rate remained the same in both the bare and modified electrodes for 10 and 20 wt.% CoO. For 5 wt.% CoO Ni solubility decreased to two-thirds of that of NiO. In our case, solubility of Ni from the modified electrode was half of that from the bare electrode. Similar results were also observed by Kuk et al. [14,15] who found that the Ni dissolution from their $LiCoO_2$-coated NiO was half of that from the untreated electrode. In our case, solubility of cobalt was about one order of magnitude smaller than that of nickel. The results indicate that cobalt deposited on NiO through electroless deposition is resistive to the molten carbonate environment. The amount of nickel and cobalt cation in the carbonate melt increases with time and saturates after about 100 h. Similar results have been obtained in the literature for the solubility of Ni^{2+} and Co^{2+} ions in the carbonate melt [18–22]. The results indicated that cobalt coating increases the barrier properties of the cathode and thereby decreases the dissolution of nickel in the melt.

3.5. Thermal oxidation behavior

In order to study the performance of the sintered electrodes under cathode gas conditions, TGA was done on the sintered nickel and cobalt-encapsulated nickel tapes. The temperature was increased from 100 to 650 °C at a rate of 10 °C/min under cathode gas atmosphere (30% CO_2 + 70% air). The temperature was then maintained at 650 °C for a period of 2 h. Fig. 5a shows the results of TGA analysis obtained for nickel tapes in the presence and absence of molten carbonate. The percentage increase in weight while heating the sample was plotted against the experiment time. The time interval between 0 and 55 min corresponds to a temperature rise from 100 to 650 °C at a heating rate of 10 °C/min. The time interval after 55 min corresponds to the period where the temperature was maintained constant at 650 °C. As shown in Fig. 5a, the weight of nickel sample in the absence of molten carbonate starts to increase after 40 min corresponding to a temperature of 400 °C and stabilizes after about 2 h at 650 °C. On the other hand, the oxidation of nickel was rapid in case of nickel sample placed

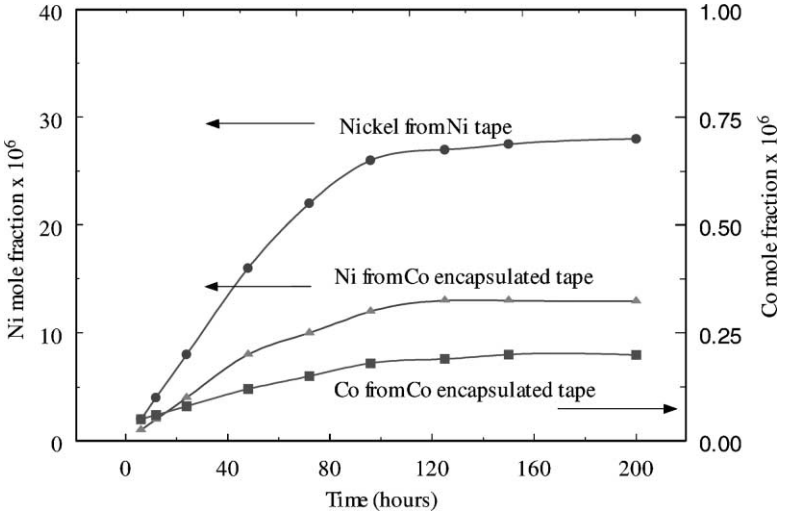

Fig. 4. Atomic absorption spectroscopy analysis of dissolved nickel and cobalt in molten carbonate melt.

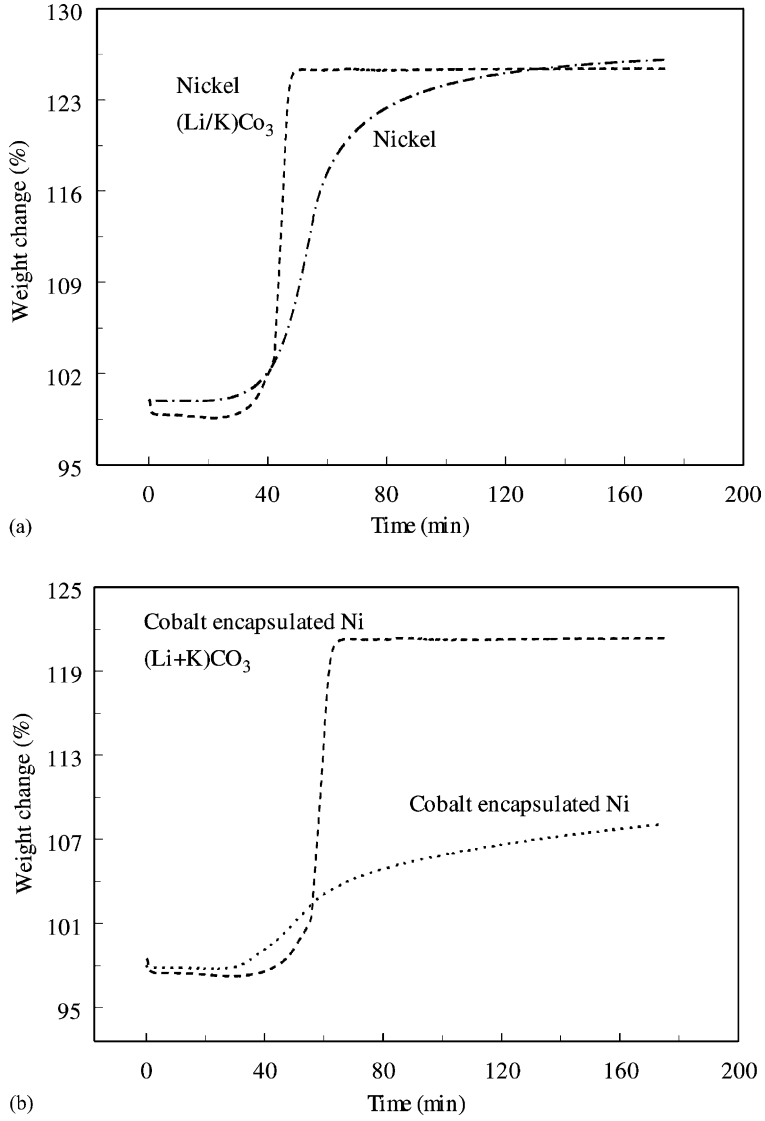

Fig. 5. TGA analysis of sintered nickel (a) and cobalt-encapsulated nickel (b) tapes under cathode gas conditions in the presence and absence of molten carbonate melt.

with molten carbonate salt in the presence of cathode gas. It appears that O_2 permeation and reaction with inner nickel particles is enhanced in the presence of molten carbonate. The weight increase in both the cases was about 27%, which suggests the complete conversion of Ni to NiO.

Oxidation of cobalt-coated nickel was very slow in the absence of molten carbonate and the oxidation continued even after 2 h after reaching 650 °C as shown in Fig. 5b. Theoretical weight increase for the conversion of Ni and Co to their oxides (NiO/CoO) based on stochiometric calculation is around 27%. In the presence of molten carbonate, weight of the cobalt-encapsulated substrate continued to increase due to oxidation and stabilized shortly after reaching 650 °C. The percentage increase in weight was around 22%. However, the actual weight increase is much lower in the absence of the carbonate melt (60% lower than with the presence of molten carbonate). This slow oxidation of cobalt-encapsulated nickel specimen is obviously due to the presence of cobalt, which is thermodynamically more stable.

3.6. Electrochemical oxidation behavior

To understand the influence of cobalt encapsulation on nickel electrode from an electrochemical point of view, the open circuit potentials of both samples were monitored as a function of time during the in situ oxidation process. Cobalt-coated sample which was sintered in air was used for this study as the objective was to study the in situ oxidation behavior. The oxidation was carried out in a three-electrode half-cell described in the Section 2 oxidant gas composition of 67% CO_2 and 33% O_2 was bubbled at a constant rate of 60 cm^3/min through an alumina tube during the in situ oxidation process. Fig. 6 compares the OCP behavior of

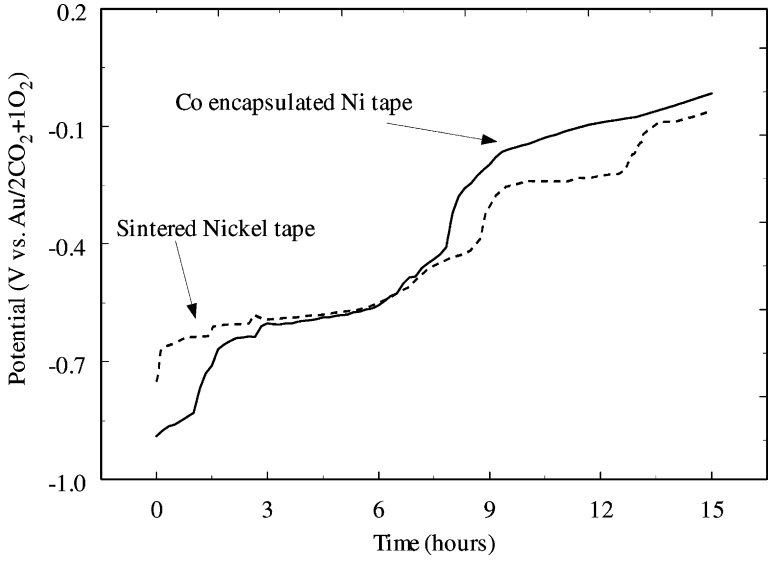

Fig. 6. Open circuit potential as a function of time during the in situ oxidation of bare and cobalt-encapsulated nickel tapes under cathode gas conditions.

bare and cobalt-encapsulated nickel electrodes as a function of immersion time.

In both cases, three different potential plateaus are observed which can be attributed to the following reactions [22,23]:

$$Ni + CO_3^{2-} \rightarrow NiO + CO_2 + 2e^- \quad -0.80\,V \tag{1}$$

$$2Ni + 3CO_3^{2-} \rightarrow Ni_2O_3 + 3CO_2 + 2e^- \quad -0.43\,V \tag{2}$$

$$Ni + CO_3^{2-} \rightarrow NiCO_3 + 2e^- \quad -0.25\,V \tag{3}$$

The first plateau in case of nickel oxidation is due to the formation of porous nickel oxide on the surface of the nickel matrix. Next, bulk nickel is oxidized to NiO at approximately −0.6 V. The second plateau at −0.44 V has been attributed to the surface oxidation of Ni(II) oxide to trivalent nickel.

The redox processes that occur during the in situ oxidation of cobalt correspond to [23,24].

$$Co + CO_3^{2-} \rightarrow CoO + CO_2 + 2e^- \quad -0.85\,V \tag{4}$$

$$3Co + 4CO_3^{2-} \rightarrow Co_3O_4 + 4CO_2 + 8e^- \quad -0.68\,V \tag{5}$$

$$Co + CO_3^{2-} \rightarrow CoCO_3 + 2e^- \quad -0.35\,V \tag{6}$$

In the case of Co-coated Ni, one can expect a solid solution of Co and Ni to be formed whose OCP is a mixed potential corresponding to oxidation of both Co and Ni.

3.7. Polarization studies

Polarization studies were carried out in a three-electrode 3 cm^2 lab scale cell containing nickel/cobalt-encapsulated nickel electrodes both as the working and counter electrodes gold (oxygen reduction) served as a reference electrode. The electrodes were separated by a $LiAlO_2$ ceramic tile containing Li–K carbonate melt (62–38 mol%). The cell is connected to a gold/oxygen reference electrode through a salt bridge. The polarization characteristics of NiO and Co–NiO cathodes were obtained by varying the current load. Fig. 7a and b compares the cathode polarization during the galvanodynamic scan for the two cathode materials as a function of different operating temperatures. The current was scanned at 1 mA/s and the curves have been corrected for IR loss based on R_Ω calculated from impedance measurements (not shown).

The i–η characteristics (Fig. 7a and b) of both NiO and Co-coated NiO are similar to each other indicating two regions; charge transfer at lower overpotentials and a complex mass transfer and charge transfer limited process at higher overpotentials. Increasing the temperature has larger influence on the polarization in case of NiO (Fig. 7a). The observed overpotentials η decrease with increasing the temperature indicating a decrease of both the polarization and diffusion overpotentials with an increase of temperature. Similar results were observed in [25,26].

As shown in Fig. 7b, similar results were also observed in case of Co-encapsulated NiO. On increasing the temperature, there is a significant change in the overpotential characteristics of Co–NiO composite. Kuk et al. [14,15] found a small improvement in the polarization performance of their $LiCoO_2$-coated NiO as compared to the untreated electrode. The observed small decrease of the overpotential when compared with the NiO overpotential in our case probably results from a small decrease of surface area of the encapsulated active material.

Reaction rate orders were obtained by performing a regression analysis of the exchange current density data obtained from i–V plots under low current load ($i \leq 10$ mA/cm^2). Fig. 8 shows the i–V plots obtained for the case of

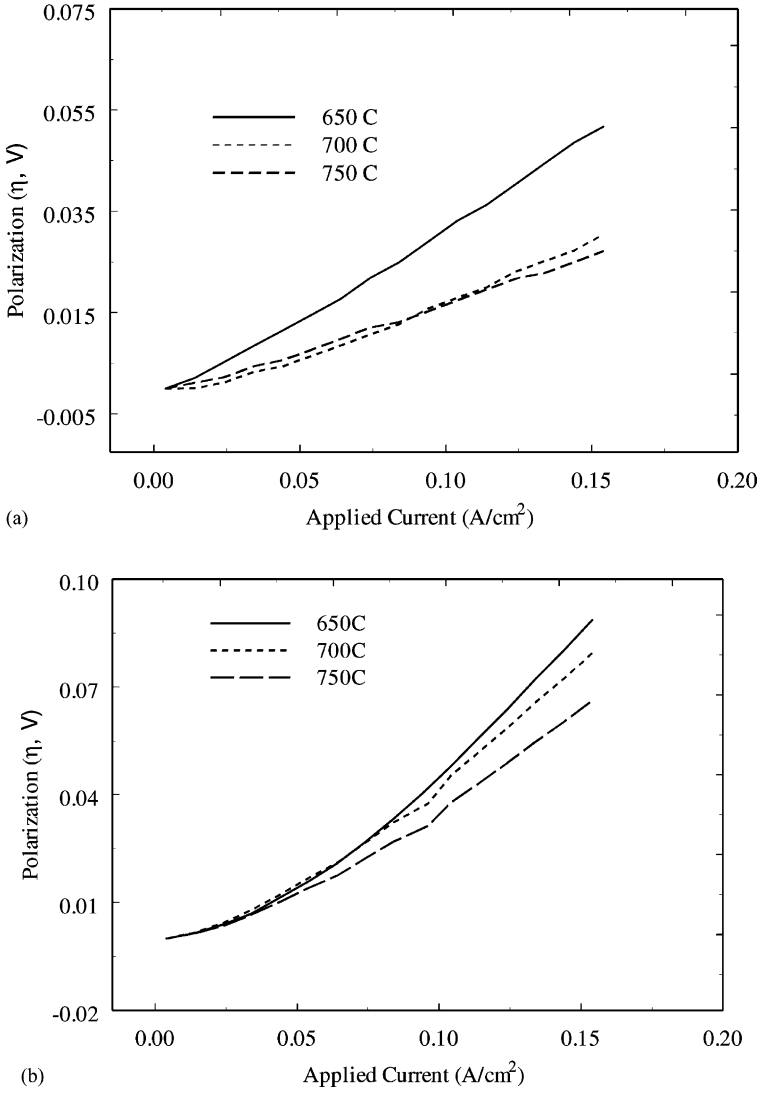

Fig. 7. Comparison of cathode polarization behavior at different current loads for bare (a) and cobalt-encapsulated nickel (b) cathodes at different temperatures.

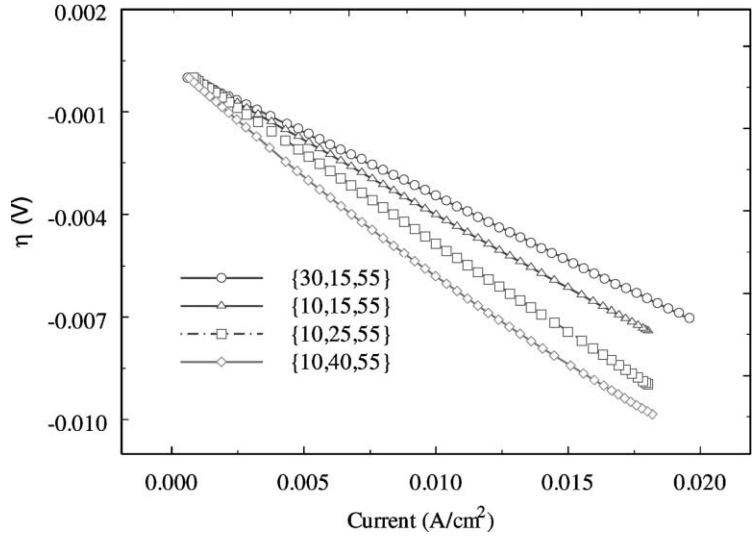

Fig. 8. Comparison of *i–V* plots obtained for CoO–NiO electrodes under different cathode gas and temperature conditions.

Co–NiO under different gas conditions. Similar studies were carried out at different temperatures and for NiO under similar conditions. The slope of the linear part of *i–V* curve was used to calculate the apparent exchange density based on the expression $i_o = RT/nFR_{ct}$, where R is the universal gas constant, T the cell temperature, F the Faraday's constant and R_{ct} is the slope of the *i–V* response. Exchange current density was estimated as a function of gas composition for Co–NiO electrode from *i–V* plots obtained at low overpotentials. Fig. 9a and b show a plot of exchange current density as a function of O_2 and CO_2 partial pressures, respectively. The slope of $\log(i_o)$ dependence with $\log(pO_2)$ is positive indicating a positive reaction order for O_2. While in the case of $\log(i_o)$ dependence versus $\log(pCO_2)$, a negative slope is observed indicating a negative reaction order for CO_2. The range of values of exchange current density calculated for Co–NiO varied from 14.2 to 16.1 mA/cm^2. The apparent exchange current density calculated using the same method for the case of NiO varied between 29 and 31 mA/cm^2. The exchange current density data offers qualitative evidence for the observed difference in polarization performance in case of Co-encapsulated and bare NiO because the *i–V* plots used to analyze the system may contain mass transfer limitations even at low current loads (due to high temperate). Thus, exchange current density data offer only a qualitative evidence for the observed difference in polarization performance in case of Co-encapsulated and bare NiO. The log plots shown in

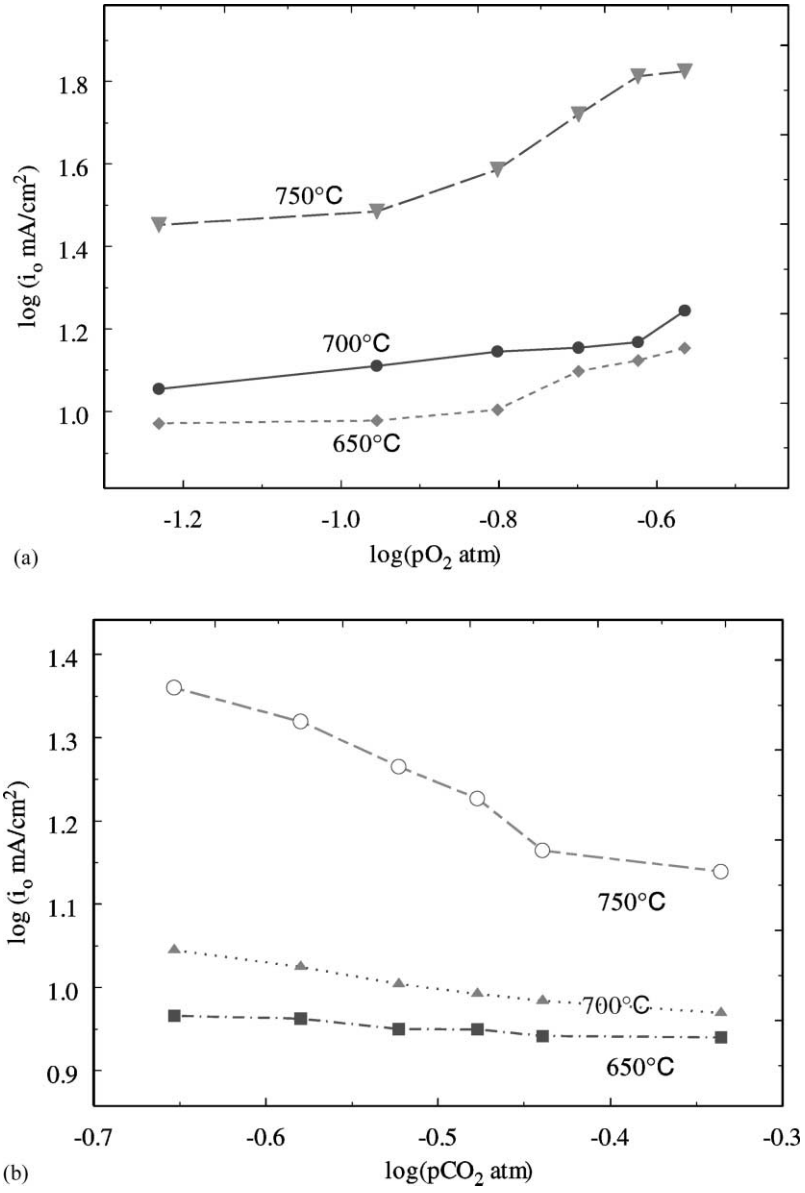

Fig. 9. Plot of apparent exchange current density of cathode reaction on cobalt-encapsulated nickel as a function of O_2 (a) and CO_2 (b) partial pressures at 650, 700 and 750 °C.

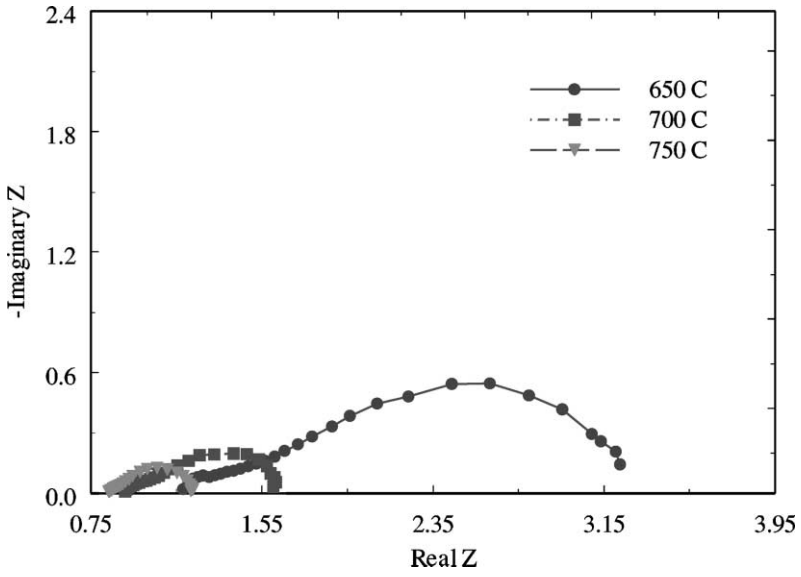

Fig. 10. Nyquist plots of impedance response of NiO electrode at different temperatures at a particular gas composition.

Fig. 9a and b were not perfectly linear implying the presence of more than one reaction mechanism. For this reason, we have not attempted to identify the observed kinetics with any particular mechanism.

3.8. Electrochemical impedance spectroscopy (EIS) studies

In order to understand further the kinetics of oxygen reduction on Co–NiO, impedance measurements were carried out at different gas compositions. EIS analysis was carried out at equilibrium potential (open circuit) on the NiO and Co–NiO electrodes. Fig. 10 shows the impedance analysis of NiO electrode at different temperatures at a particular gas composition. The impedance response at any given temperature is characterized by the presence of high frequency loop and an extension at low frequencies. The high frequency plot has been associated with the charge transfer processes while the low frequency loop to a slow process (mass transfer or slow homogeneous reactions). The impedance response shown in Fig. 10 is similar in appearance to the ones obtained by Yuh and Selman [25,26] under similar conditions. As shown in Fig. 10, the cell temperature has a marked effect on the ac impedance. Increasing the temperature, a drastic decrease is observed in Fig. 10 of charge transfer resistance, which is in agreement with the results obtained from polarization studies.

Fig. 11a and b show the impedance response of Co–NiO electrode as a function of different gas compositions at two different temperatures. The impedance responses appear differently in case of Co–NiO when compared to those of NiO. The two distinct loops occurring at high and low frequencies in the case of NiO appear to be merged with each other in case of Co–NiO. The effect of temperature clearly shows that the observed depressed semi-circle loop includes both the charge transfer and mass transfer phenomenon. At higher temperature, the total impedance as acquired from the Nyquist plots decreases suggesting that the observed effect could well be assumed as a combination of mass transfer and charge transfer. From Fig. 11a and b, it can also be seen that the effect of partial pressure of O_2 and CO_2 are antagonistic to each other. The magnitude of the impedance loop decreased on increasing the O_2 partial pressure. This clearly indicates a positive reaction order for oxygen and is similar to the response seen for NiO [26]. In case of CO_2, the impedance value increased with an increase in CO_2 partial pressures implying that the reaction order of CO_2 must be negative. Yuh et al. [26] obtained similar results for NiO in terms of O_2 and CO_2 dependence on impedance responses.

3.9. Post-test characterization

EDAX analysis was carried out to characterize the cobalt content in the cobalt-encapsulated cathodes after 72 and 300 h of polarization. EDAX patterns were identical in both cases. The concentration calculations based on the intensity peaks show that the cobalt and nickel concentration remain the same however, conclusions cannot be made about the long-term performance of this material based on this observation. The rate of dissolution was comparatively lower in case of Co–NiO when compared to that of NiO as shown in Fig. 4. X-ray diffraction (XRD) studies were carried out on post-test Ni and Co–NiO cathode samples to identify the changes due to interaction in molten carbonate. Fig. 12 shows the XRD pattern of nickel and cobalt-coated nickel cathodes treated in molten carbonate under cathode gas conditions for a period of 300 h. XRD pattern of Ni tape is characterized by peaks corresponding to NiO, while that of Co–NiO shows a different pattern due to the presence of mixed oxides.

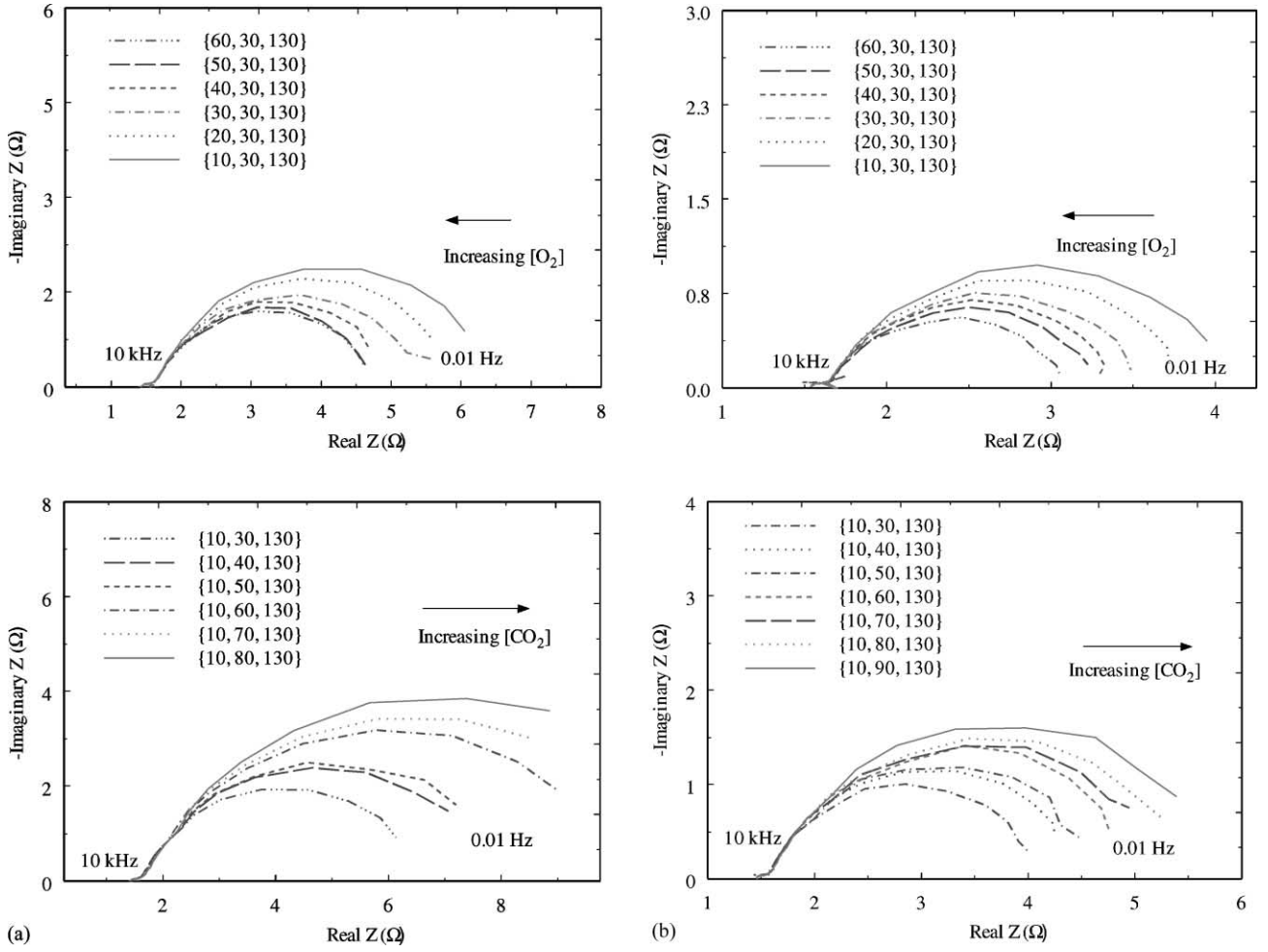

Fig. 11. Nyquist plots of impedance response of cobalt-encapsulated nickel electrode as a function of O_2 and CO_2 partial pressures at 650 °C (a) and 700 °C (b). The numbers in parenthesis "{}" indicates the O_2, CO_2 and N_2 concentrations in cm^3/min.

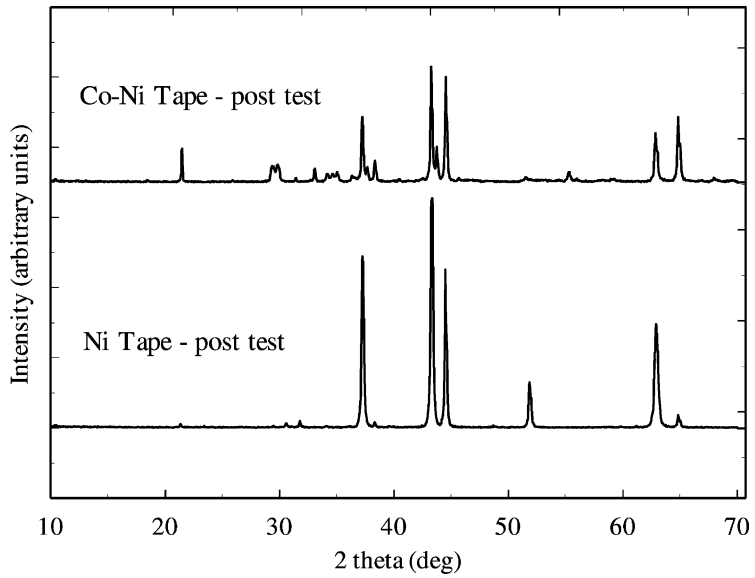

Fig. 12. XRD patterns of NiO and Co–NiO cathodes treated in molten carbonate under cathode gas conditions for a period of 300 h.

4. Conclusion

Nickel cathodes for MCFC were made by a tape casting and sintering process. Subsequently, they were treated using a surface modification technique wherein a thin film of cobalt was formed over the sintered tape. SEM analysis on nickel and cobalt-encapsulated nickel electrodes show morphological changes in case of cobalt-coated electrodes. It was found that cobalt-coated electrodes have a lower solubility in the molten carbonate melt when compared to bare nickel electrodes in the presence of cathode gas conditions. The solubility decreased more than 50% due to microencapsulation with cobalt. The Co–NiO, thermal oxidation rate was much lower in case of cobalt-encapsulated electrode. The *i–V* characteristics and polarization behavior for Co-encapsulated NiO are different from that of NiO. A small increase in polarization in case of Co–NiO was seen to be due to reduced exchange current density. Impedance spectroscopic studies do not indicate any change in mechanism in case of Co–NiO when compared to NiO. Co–NiO composite can be regarded as an alternative cathodes for MCFC. This composite improves the corrosion properties of conventional nickel oxide cathodes in MCFC.

Acknowledgements

Financial support by the National Energy Technology Laboratory (NETL), which is supported by the US Department of Energy (DOE), is gratefully acknowledged.

References

[1] A.J. Appleby, F.R. Foulkes, Fuel Cells Handbook, Von Nostrand Reinhold, New York, 1989.
[2] K. Joon, J. Power Sources 71 (1998) 12.
[3] J.R. Selman, in: S.S. Penner (Ed.), Assessment of Research Needs for Advanced Fuel Cells by the DOE Advanced Fuel Cell Working Group (AFCWG), Permagon Press, New York, 1984.
[4] T.G. Benamin, E.L. Camara, L.G. Marianowski, Handbook of Fuel Cell Performance, Contract No. EC-77C-03-1545, Chicago, IL, 1980.
[5] L. Christner, L. Paetsch, P. Patel, M. Farooque, Scale-up of internal reforming molten carbonate fuel cells, in: Proceedings of the 1988 Fuel Cell Seminar, Long Beach, CA, 1988, p. 403.
[6] K. Tanimoto, Y. Miyazaki, M. Yanagida, S. Tanase, T. Kojima, N. Ohtori, H. Okuyama, T. Kodama, Denki Kagaku 59 (7) (1991) 619.
[7] K. Tanimoto, Y. Miyazaki, M. Yanagida, T. Kojima, N. Ohtori, T. Kodama, Denki Kagaku 63 (4) (1995) 316.
[8] L. Plomp, E.F. Sitters, C. Vessies, F.C. Eckes, J. Electrochem. Soc. 138 (2) (1991) 629.
[9] L. Giorgi, M. Carewska, S. Scaccia, E. Simonetti, F. Zarzana, Denki Kagaku 64 (6) (1996) 482.
[10] C. Lagergren, A. Lundblad, B. Bergman, J. Electrochem. Soc. 141 (11) (1994) 2959.
[11] T. Fukui, S. Ohara, H. Okawa, T. Hotta, M. Naito, J. Power Sources 86 (2000) 340.
[12] T. Fukui, H. Okawa, T. Hotta, M. Naito, T. Yokayama, J. Am. Ceram. Soc. 84 (2001) 233.
[13] X. Zhang, H. Okawa, T. Fukui, Denki Kagaku 66 (11) (1998) 1141.
[14] S.T. Kuk, Y.S. Song, K. Kim, J. Power Sources 83 (1999) 50.
[15] S.T. Kuk, Y.S. Song, S. Suh, J.Y. Kim, K. Kim, J. Mater. Chem. 11 (2001) 630.
[16] B.S. Haran, B.N. Popov, R.E. White, J. Electrochem. Soc. 145 (1998) 3000.
[17] P.L. Mangonon, Principles of Materials Selection for Engineering Design, Prentice Hall, Englewood Cliffs, NJ, USA, 1999, p. 173.
[18] K. Tanimoto, Y. Miyazaki, M. Yanagida, S. Tanase, T. Kojima, N. Ohtori, H. Okuyama, T. Kodama, Denki Kagaku 59 (7) (1991) 619.
[19] K. Ota, S. Mitsushima, S. Katao, S. Asano, H. Yoshitake, N. Kamiya, J. Electrochem. Soc. 139 (3) (1992) 667.
[20] X. Zhang, P. Capobianco, A. Torazza, B. Passalacqua, Electrochemistry 67 (6) (1999).
[21] J.B.J. Veldhuis, F.C. Eckes, L. Plomp, J. Electrochem. Soc. 139 (1) (1992) L6.
[22] K. Ota, Y. Takeishi, S. Shibata, H. Yoshitake, N. Kamiya, J. Electrochem. Soc. 142 (10) (1995) 3322.
[23] P. Tomczyk, H. Sato, K. Yamada, T. Nishina, I. Uchida, J. Electroanal. Chem. 391 (1995) 133.
[24] B.Y. Yang, K.Y. Kim, Electrochim. Acta 43 (1998) 3343.
[25] C.Y. Yuh, J.R. Selman, J. Electrochem. Soc. 138 (12) (1991) 3642.
[26] C.Y. Yuh, J.R. Selman, J. Electrochem. Soc. 138 (12) (1991) 3649.